

Interplay of coupling, residual, and quasiparticle losses for the frequency- and temperature-dependent quality factor of superconducting resonators

Elies Ben Achour, Cenk Beydeda, Gabriele Untereiner,
Martin Dressel, Marc Scheffler

1. Physikalisches Institut, Universität Stuttgart, Pfaffenwaldring 57,
70569 Stuttgart, Germany

E-mail: marc.scheffler@pi1.physik.uni-stuttgart.de

12 December 2024

Abstract. The overall, loaded quality factor Q_L quantifies the loss of energy stored in a resonator. Here we discuss on general grounds how Q_L of a planar microwave resonator made of a conventional superconductor should depend on temperature and frequency. We consider contributions to Q_L due to dissipation by thermal quasiparticles (Q_{QP}), due to residual dissipation (Q_{Res}), and due to coupling (Q_C). We present experimental data obtained with superconducting stripline resonators fabricated from lead (Pb), with different center conductor widths and different coupling gaps. We probe the resonators at various harmonics between 0.7 GHz and 6 GHz and at temperatures between 1.5 K and 7 K. We find a strongly frequency- and temperature-dependent Q_L , which we can describe by a lumped-element model. For certain resonators at lowest temperatures we observe a maximum in the frequency-dependent Q_L when Q_{Res} and Q_C match, and here the measured Q_L can exceed 2×10^5 .

Keywords: superconducting microwave resonators, resonator coupling, superconducting properties of Pb, electrodynamic of superconductors, stripline resonators

1. Introduction

Planar superconducting microwave resonators play an important role in basic and applied research [1, 2]. One prominent direction is coupling GHz photons to solid-state quantum bits for fundamental quantum optics studies and for applications in quantum computing [3, 4]. Another one employs superconducting resonators as sensitive detectors for photons or particles [5]. Most popular resonator designs are either based on coplanar waveguides (CPWs) or on lumped element circuits; in both cases the microstructure fabrication requires just a single superconducting layer. Traditionally, a few well-established superconductors such as Al, Nb, or NbN are used for this purpose. More recently, there is increased interest in a variety of other candidate superconductors. One motivation is tuning the superconducting energy gap for low-energy photon detection [6]. Another is employing high kinetic inductance, as found in strongly disordered or granular superconductors [7], for novel quantum circuitry [8–10]. Yet another motivation is mitigating material-induced noise in quantum devices [11, 12]. Towards this goal, residual absorption in the bulk as well as at surfaces and interfaces has to be reduced, and here alternative superconductors such as Ta have been investigated [13]. For all the mentioned applications, superconducting microwave resonators are usually operated at mK temperatures, much lower than the critical temperature T_c .

The strong interest to improve superconductors for various GHz applications converges with another well-established research direction: planar microwave resonators are used to study fundamental electrodynamic properties of various material classes, including superconductors [14–19]. From such a microwave spectroscopy perspective, one is usually interested in probing the bulk response of a material of interest as function of temperature [20–23], ideally also as function of frequency [15, 17, 24–26], and often as a function of magnetic field [16, 27–30]. For such experiments, the studied material could either constitute a core element of the resonator [31, 32] or act as a perturbation to a well-characterized resonator [33–36].

The goal of the present study is bringing together concepts of superconducting planar resonators from quantum circuitry and microwave spectroscopy: we characterize multi-mode resonators towards their limits in quality factor imposed by coupling, thermally induced quasiparticles, and residual losses. This might offer new perspectives in several regards: (1) We employ superconducting stripline (triplate) resonators. These are more difficult to fabricate than e.g. CPW resonators, but they have very low radiative losses and are convenient if one wants to probe a bulk sample of a conductor [14, 16, 17, 37]. (2) The resonators

are made of lead (Pb), which is a conventional superconductor with substantial $T_c = 7.2$ K, has low kinetic inductance, and can be fabricated easily as thin films via thermal evaporation. The low-energy properties of superconducting Pb have been studied carefully and act as benchmarks for the fundamentals of BCS theory [38–43]. Furthermore, early microwave studies indicated rather low residual losses [44–46], and for spectroscopic studies in magnetic field the type-I superconductivity of Pb with highest critical field of 80 mT can be helpful [47, 48]. (3) We explicitly address the frequency dependence [14, 17, 49], which is highly relevant for spectroscopy, and we focus on the range from 0.7 GHz to 6 GHz, which overlaps with the conventional operating range of quantum circuits and detectors. (4) We cover temperatures from 1.5 K to 7 K, i.e. from temperatures where thermally excited quasiparticles can be neglected in terms of losses until they fully dominate losses close to T_c .

2. Temperature and Frequency Regimes of Q_L

The frequency-dependent response of a resonator is often described with the Lorentz model [50]

$$y(f) = \frac{A}{f - f_0 + if_b/2} \quad (1)$$

where A is the amplitude, f the frequency, f_0 the resonance frequency and f_b the full width at half maximum (FWHM). For the superconducting transmission line resonators used in this work, $y = S_{21}$ is the forward scattering coefficient. The loaded quality factor

$$Q_L = \frac{f_0}{f_b} \quad (2)$$

can be understood as the ratio of energy stored to the energy lost per cycle in a resonator. Q_L can be straightforwardly extracted from a measurement. Losses in a resonator add up linearly in f_b , but it is common to subdivide the loaded quality factor Q_L into the different loss mechanisms that contribute to Q_L . For our case of a superconducting stripline resonator, we distinguish losses through the coupling Q_C , losses due to thermally excited quasiparticles in the superconductor Q_{QP} , and residual losses Q_{Res} :

$$\frac{1}{Q_L} = \frac{1}{Q_C} + \frac{1}{Q_{QP}} + \frac{1}{Q_{Res}}. \quad (3)$$

Here we assume that dielectric losses in the sapphire substrate and radiation losses in a stripline geometry are negligible. We also neglect the pair-breaking contribution to Q_L since we probe the resonators at frequencies much lower than the energy gap $hf \ll 2\Delta_0$.

In figure 1 it can be seen which loss mechanism is expected to dominate in such a superconducting

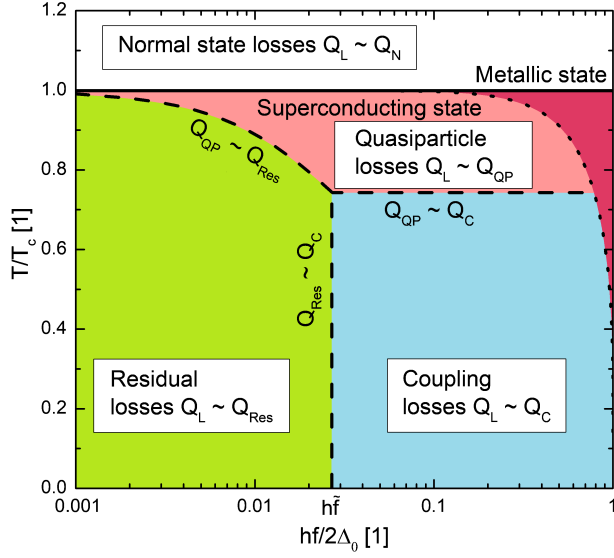


Figure 1. Schematic regimes in temperature T (normalized to the critical temperature T_c) and frequency f (normalized to the superconducting energy gap $2\Delta_0$ at zero temperature, with h Planck's constant) concerning different loss mechanisms in a superconducting resonator. The loaded quality factor Q_L in the superconducting state is dominated by residual losses (quantified by Q_{Res}), coupling losses (Q_C), or thermally excited quasiparticles (Q_{QP}), while above T_c losses due to normal-conductive electrons (Q_N) dominate. The dotted line denotes the temperature dependence of the energy gap $2\Delta(T)$, which introduces an additional pair-breaking contribution to Q_L for frequencies $f > 2\Delta(T)/h$. The cross-over frequency \tilde{f} indicates where the dominant source of losses changes from residual to coupling losses. For details on the shape of the dashed line for $Q_{\text{QP}} \sim Q_{\text{Res}}$, see Appendix A.

resonator for given temperature T and frequency f . At temperatures close to T_c the superconducting resonator performance is governed by absorption due to the substantial density of thermally excited quasiparticles ($Q_{\text{QP}} \propto 1/f$). Upon further cooling, the loss mechanism changes depending on the frequency f . For low frequencies, the resonator performance is limited by residual losses ($Q_{\text{Res}} \propto f$), which persist even at lowest temperatures. Those residual losses result from imperfections in the resonator geometry, or from residual non-superconducting quasiparticles that are not covered by the Mattis-Bardeen formalism [51] to describe optical absorption of conventional superconductors based on the BCS theory. For sufficiently high frequency the losses are determined by the resonator coupling ($Q_C \propto 1/f$), because the impedance of the resonator coupling gap decreases resulting in a stronger leakage through the gap.

The highest quality factor in such a resonator is achieved by a trade-off between residual losses and coupling losses, for a frequency \tilde{f} at which $Q_{\text{Res}} \sim Q_C$. It is possible to probe this trade-off experimentally by employing multi-mode resonators at several resonance

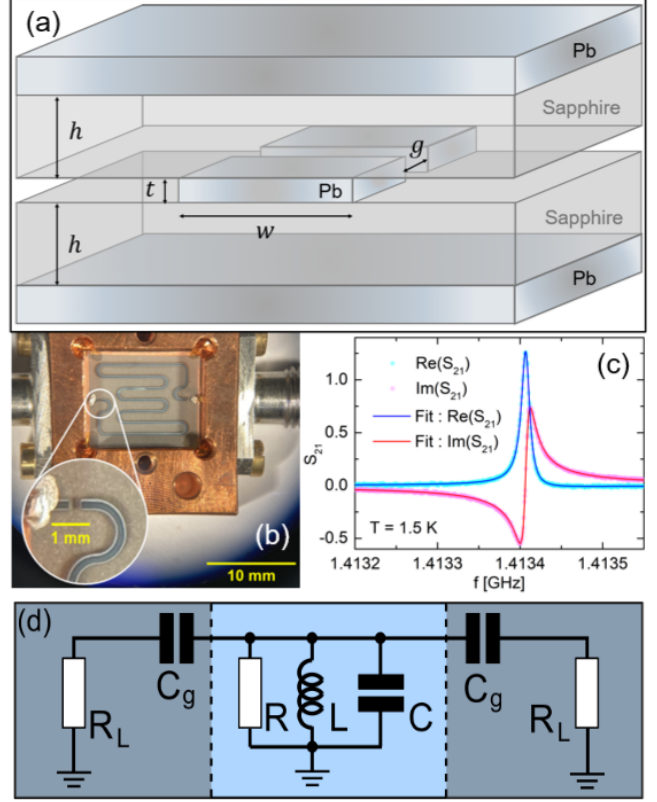


Figure 2. (a) Scheme of a stripline transmission line as used for resonators, with the definition of relevant geometrical parameters. (b) Photograph of the copper box that contains the resonator without the upper sapphire substrate and ground plane. The gray bent line is the center conductor. As shown in the zoomed zone, the center conductor is gapped at two locations such that the center conductor has a finite length l . The length g of the gap in the inner conductor is here $300 \mu\text{m}$. (c) Complex components of S_{21} for resonator 4 around the second resonant mode at $T = 1.5 \text{ K}$. The solid lines are the results of the fit of the data points using equation (5). The amplitude of the signal exceed unity because an amplifier was used to raise the magnitude of the output signal. (d) Lumped-element circuitry used to model the resonances: the actual resonator are the elements in the blue-shaded middle section, whereas the gray-shaded sections represent the coupling to the environment.

frequencies at lowest temperature.

3. Experimental Techniques

In our setup a resonator is a transmission line of finite length l made of Pb. The length of the transmission line results in a discrete set of resonance frequencies

$$f_n = \frac{nc}{2l\sqrt{\epsilon_r}}, \quad n \geq 1 \quad (4)$$

with a Lorentzian shape in transmission, where ϵ_r is the permittivity of the sapphire dielectric and c the speed of light in vacuum. Here we have neglected the contribution of the kinetic inductance of the Pb superconductor. A measurement of the

N°	Type	l (cm)	h (μm)	w (μm)	g (μm)	$f_{0,\text{des}}$ (GHz)	$f_{0,\text{exp}}$ (GHz)	$Q_L \cdot 10^{-3}$	C_g (fF)
1	A	5	430	155	60	0.95	0.87	15.0	17.8
2	A	5	430	155	150	0.95	0.89	87.0	7.5
3	A	5	430	155	300	0.95	0.95	90.3	6.3
4	B	6	127	45	30	0.79	0.71	115.7	6.6
5	B	6	127	45	100	0.79	0.72	206.9	4.0

Table 1. Overview of the five studied resonators: Relevant geometric parameters as presented in figure 2 are resonator length l , height h of the dielectric between center conductor and ground planes, and width w of the center conductor. The height $t = 1 \mu\text{m}$ of the center conductor is the same for all resonators. The length of the gaps g in the center conductor determines the coupling capacitance C_g , which we determine from the experimental data at base temperature. The resonance frequency of the fundamental mode is designed as $f_{0,\text{des}}$ and found experimentally as $f_{0,\text{exp}}$ at base temperature of 1.5 K. The observed loaded quality factor Q_L at base temperature is given for the second resonance mode at 1.7 GHz and 1.4 GHz, respectively, for type A and type B geometry.

broadband transmission spectrum of this resonator returns equidistantly spaced transmission peaks of several harmonic modes. Our experimental setup imposes resonator lengths of a few centimeters, leading to fundamental modes in the microwave range around 1 GHz. The meander-shaped resonator structure can be seen in figure 2(b). The impedance mismatch due to the curvature of the conductor is negligible if the radius of curvature is at least three times larger than the width w of the inner conductor [52].

In figure 2(a) the cross-section of the transmission line can be seen. We use a stripline geometry with an inner conductor of width w and thickness t that is sandwiched between two ground plates where the lower ground plate is $6 \mu\text{m}$ and the upper ground plate $1 \mu\text{m}$ thick. Both ground plates share the same electrical potential, the center conductor is electrically isolated from the ground plates by two layers of sapphire with thickness h . The center conductor is fabricated by evaporating Pb onto sapphire using a mechanical shadow mask, the upper ground plate is also evaporated on sapphire whereas the lower ground plate consists of a Pb foil. The center conductor has two gaps with length g , as it can be seen in figure 2(b). The coupling via the gap can be described effectively by a capacitance C_g , which should depend on the geometry of the resonator. The resonator structure is mounted in a brass or copper box that shields the resonator and enables electric contact between the two ground plates. The metal box contains two SMA or 1.85 mm connectors that are connected to the stripline center conductor with silver paste.

For this study, we use five stripline resonators with different geometry parameters, as listed in table 1, in order to vary the coupling capacitance value C_g . These parameters are chosen such that the length of the coupling gap g varies over a wide range. However, it is always kept smaller than the thickness h of the substrate, $g < h$, to prevent coupling via the ground plates. Therefore, we use two types of geometries with different h : type A with $h = 430 \mu\text{m}$ and type B with $h = 127 \mu\text{m}$. Furthermore, since the

characteristic impedance Z_0 of the transmission line is fully determined by the ratio w/h of the center conductor width and the substrate thickness [53], the width w is adjusted for each resonator type to match the characteristic impedance to 50Ω .

The resonators are placed in a cryostat with base temperature below 1.5 K [54] and connected to a two-port vector network analyzer (VNA) via coaxial cables that measures the spectrum of the resonators from 300 kHz to 20 GHz. Typical applied microwave powers are around -40 dBm. We measure at temperatures $1.5 \text{ K} < T < 8 \text{ K}$ and record for each resonator mode the microwave transmission spectrum S_{21} with high resolution. The measured complex components of S_{21} at resonance are fitted for each temperature, allowing to extract the resonant frequencies and the corresponding FWHM. We use the fitting function

$$S_{21}^{\text{fit}}(f) = e^{2\pi i f \tau} \left(\frac{A}{f_b/2 + i(f - f_0)} + a + b(f - f_0) \right). \quad (5)$$

The complex parameters a and b model a linear background in the signal. The real coefficient τ accounts for a phase shift between the real and the imaginary parts of the signal, which often occurs, due to some phase delay induced by the cables. The inset in figure 2(c) presents the result of this fitting procedure for an exemplary resonance.

4. Analysis

The quality factors of the resonance modes can be extracted from the measured spectra for every set temperature. The different resonators span a substantial range of accessible Q_L , as can be seen from table 1, where the value for Q_L for the second resonance mode at $T = 1.5 \text{ K}$ is given for each resonator. Figure 3 shows the frequency dependence of the quality factor at different temperatures for two resonators of different type. These dependences seem to be similar at highest temperatures and frequencies but not for low temperature and frequency, where the data points form a maximum around 1 GHz for

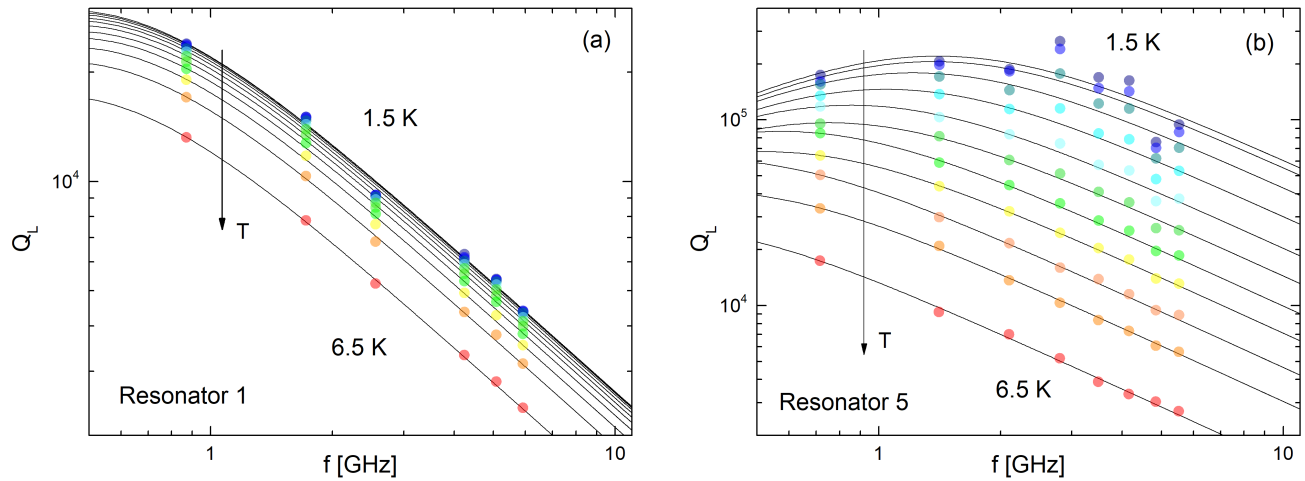


Figure 3. Loaded quality factor Q_L as a function of frequency f for temperatures from 1.5 K to 6.5 K with increment of 0.5 K for resonator 1 in panel (a) and resonator 5 in panel (b). The continuous lines correspond to the fit of the data points using equation (10) for each temperature independently. All resonators of a given type (A or B) have similar frequency and temperature dependence of their quality factor. Both type A and B resonators show the same behavior at high frequency but type B resonators, with thinner substrate, feature a maximum at low frequency (around 1 GHz for resonator 5).

resonator 5. This would suggest that there exist at least two relevant loss mechanisms that exhibit different frequency dependence.

To investigate this, we use a lumped-element model for the resonators as presented by Göppl *et al.* in [1], and shown in figure 2(d). This model supposes that the transmission line of length l can be modeled as a parallel RLC circuit near resonance and for small losses. It defines an internal quality factor

$$Q_{\text{int}} = \omega_n RC \quad (6)$$

with resonant frequencies $\omega_n = n \cdot 2\pi f_0 = n(LC)^{-1/2}$. The inductance L and capacitance C can be computed knowing the geometry of the transmission line, and R is a resistance that models the internal losses. Assuming symmetric coupling gaps and a low coupling regime ($\omega_n R_L C_g \ll 1$) one can quantify a coupling quality factor [1]

$$Q_C = \frac{C}{2\omega_n R_L C_g^2} \quad (7)$$

where $R_L = 50 \Omega$ is the impedance imposed by the VNA and the connecting coaxial cables, and C_g is the coupling capacitance. The loaded quality factor is the parallel association of these two quality factors, such that:

$$Q_L^{-1} = Q_{\text{int}}^{-1} + Q_C^{-1} \quad (8)$$

In this model, the only unknown parameters are the coupling capacitance C_g and the resistance R . The latter is inversely proportional to the surface resistance R_S of Pb, which is a function of frequency and temperature. In our frequency regime, it had been predicted and measured [17, 55] that the surface

resistance has the approximate form

$$R_S(\omega, T) = \rho_S(T)\omega^2 + R_{\text{Res}}(T) \quad (9)$$

where $\rho_S(T)$ quantifies the losses due to thermally excited quasiparticles and would only be a function of temperature. R_{Res} models the possible residual losses due to Pb itself, due to geometrical defects in the structure, or due to unknown loss mechanisms. Therefore, equations (6)-(9) would lead to the following form for the loaded quality factor:

$$Q_L^{-1} = \alpha(T)f + \beta(T)\frac{1}{f} \quad (10)$$

with

$$\alpha(T) = kC_g^2 + k'\rho_S(T) \quad (11)$$

$$\beta(T) = k'R_{\text{Res}}(T) \quad (12)$$

where k and k' are two parameters that can be computed: k accounts for the contribution of the coupling losses to Q_L , and k' quantifies how intrinsic loss mechanisms of the resonator affect Q_L . In this study one only needs to compute $k = 4\pi R_L / C$, where C is obtained using conformal mapping [53]. For the two different resonator types we obtain $k(\text{type A}) = 1.2 \times 10^{14} \Omega \text{F}^{-1}$ and $k(\text{type B}) = 1.0 \times 10^{14} \Omega \text{F}^{-1}$, respectively. The final form for the loaded quality factor in equations (10)-(12) leads to equation (3) where $Q_C^{-1} = kC_g^2 f$, $Q_{\text{QP}}^{-1} = k'\rho_S f$ and $Q_{\text{Res}}^{-1} = k'R_{\text{Res}}/f$. The highest quality factor according to equation (10) occurs for every temperature at a cross-over frequency $\tilde{f}(T) = \sqrt{\beta(T)/\alpha(T)}$.

At high frequency $f > \tilde{f}$, according to equation (10), one would have $Q_L(f > \tilde{f}) \propto f^{-1}$.

In this regime, the losses are dominated both by the quasiparticles and the external coupling, where the ratio between the two depends on the temperature. Close to T_c , the large number of quasiparticle excitations results in a rise of the surface resistance which lowers Q_{QP} , therefore the quasiparticle loss dominates the loaded quality factor $Q_L \sim Q_{QP}$. For low temperatures (and again $f > \tilde{f}$), coupling losses dominate $Q_L \sim Q_C$. In principle, the coupling loss should be temperature independent. Thus, for determining the coupling capacitance, one will suppose that $\rho_S(T) \rightarrow 0$ at base temperature of 1.5 K, such that Q_L is given by C_g in this regime. The crossover from $Q_L \sim Q_{QP}$ to $Q_L \sim Q_C$ upon cooling at high frequency cannot be extracted from the frequency dependence of Q_L , since both Q_{QP} and Q_C are anti-proportional to frequency. With respect to figure 1, it corresponds to the crossing of the dashed line from the pink zone to the blue one.

5. Experimental Results

The transition from the low-frequency dependence $Q_L(f < \tilde{f}) \propto f$ to the high-frequency dependence $Q_L(f > \tilde{f}) \propto f^{-1}$ is visible for resonator 5 in figure 3 around 1 GHz, for the lowest temperatures only. The quasiparticle losses contribution is negligible at base temperature. Thus, the relevant loss mechanisms are the residual and the external coupling losses. For sufficiently small coupling losses at low frequency, the residual losses dominate $Q_L \sim Q_{Res}$, resulting in a linear frequency dependence of Q_L . This would suggest that resonator 1 shows stronger coupling than resonator 5, since \tilde{f} is shifted to lower frequencies (resulting from higher $\alpha \sim C_g^2$ at low T).

For higher temperature, the quasiparticle losses rise (α increases), resulting in \tilde{f} shifting to lower frequencies. Thus, for all resonators at high temperatures the cross-over frequency does not appear in our frequency window, since Q_{QP} will be always smaller than Q_{Res} .

Using equation (10), the frequency dependence of Q_L is fitted, with α and β as fit parameters. The result of these fits are plotted as black lines in figure 3. Each curve corresponds to a fixed temperature and is obtained independently. The resulting fit parameters α and β are plotted as function of temperature for all five resonators in figure 4(a) and 4(c), respectively.

These parameters allow us to access different physical quantities of interest. First, assuming that $\rho_S(T) \rightarrow 0$ at base temperature, $\alpha(T \rightarrow 0)$ gives a value of C_g for each resonator. The results for these measurements are given in table 1. One can observe here that a smaller cross-section of the inner conductor results in a lower coupling capacitance and that (for a

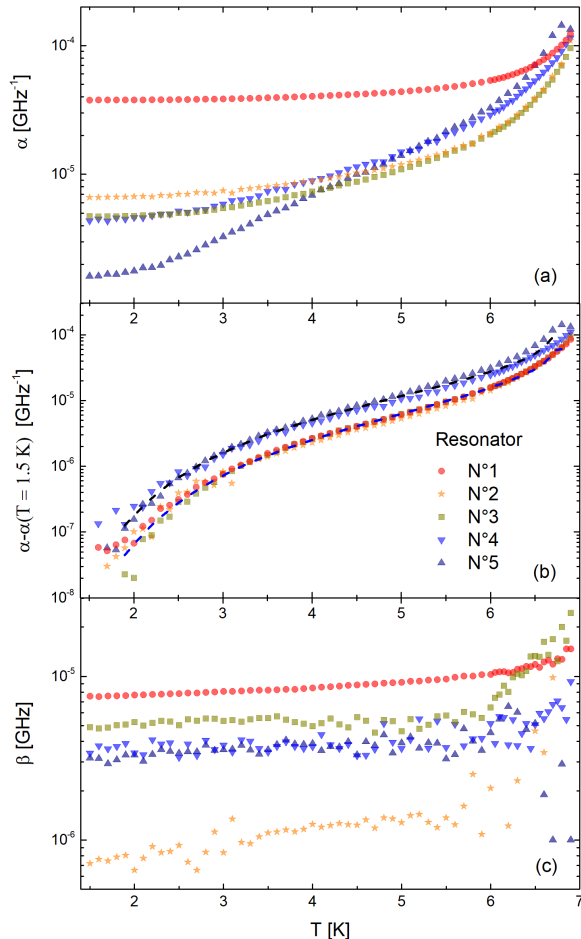


Figure 4. Resulting fit parameters α and β from the fit with equation (10) to the frequency-dependent Q_L for each temperature and for the five resonators. The parameter α in (a) accounts for the quasiparticle losses through the temperature-dependent ρ_S and the temperature-independent coupling losses. One assumes that $\rho_S \rightarrow 0$ at base temperature of 1.5 K, allowing to estimate the coupling capacitance C_g . Panel (b) shows $\alpha(T) - \alpha(T = 1.5 \text{ K})$ for the five resonators, which separate into two bundles corresponding to two resonator types. The fits are based on the expected temperature dependence of the surface resistance, see Appendix B for details. The parameter β in (c) is directly proportional to the residual losses modeled by the resistance R_{Res} .

given type of resonator) C_g is a decreasing function of the gap length g . Both of these observations are consistent with the behavior of a planar capacitance with respect to its geometry. However, for similar ratio tw/g , the capacitance is lower for smaller h , as the results for resonator 3 and 5 can show. Therefore, the parameter h should play a role for the coupling capacitance, which seems reasonable since its order of magnitude is similar to those for g or w .

A second physical parameter that can be discussed is the temperature dependence of the surface resistance R_S of Pb, encoded in the quantity $\rho_S(T)$, see equation (9). This quantity seems to reach higher values

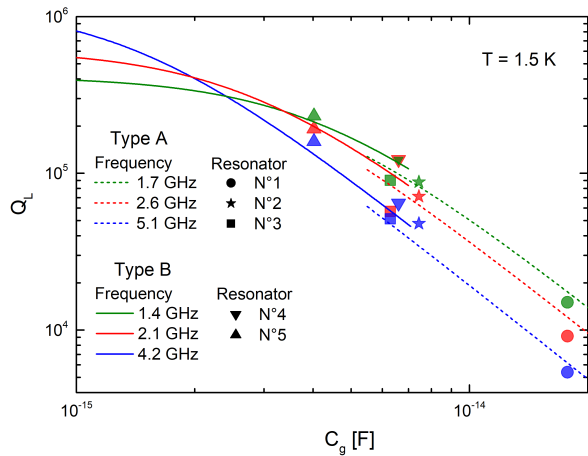


Figure 5. Quality factor dependence with respect to the coupling capacitance for resonance modes 2 (green), 3 (red) and 6 (blue) at $T = 1.5$ K. The solid and dashed lines are obtained from fitting the frequency dependence of Q_L and by inserting a continuous range for C_g in equation (10). Type A and B have different length, therefore the resonances occur at different frequency.

as the temperature gets closer to T_c . Indeed, a higher density of thermally excited quasiparticles is expected for increasing temperature, and even more so upon approaching T_c and thus shrinking of the superconducting energy gap. This behavior can be quantitatively studied through the quantity $\alpha(T) - \alpha(T = 1.5 \text{ K})$, see figure 4(b), which is proportional to $\rho_s(T)$. These experimental data are fitted separately for each resonator type and show good agreement with the prediction of the temperature dependence of $R_s(\omega, T)$ [55], see Appendix B for details.

The residual losses measurements suggest that R_{Res} is temperature independent, as evident from the almost constant values of β for the five resonators in figure 4(c). However, the substantial scattering of the measurements for different resonators could indicate that the measured parameter R_{Res} is not intrinsic to Pb but linked to other loss mechanism due, for instance, to the fabrication of the resonators.

In figure 5 the total quality factor Q_L is plotted with respect to the coupling capacitance. The data points in figure 5 correspond to modes 2, 3 and 6 at $T = 1.5$ K for each resonator, the solid and dashed lines account for the 2 different lengths l of the resonator types. The lines result from equation (10) with varying C_g and by plugging in a single value of β for each resonator type. These values were obtained from averaging the results for β , at lowest temperature, across the resonators of a given type [$\beta(\text{type A}) = 4.4 \times 10^{-6}$ GHz and $\beta(\text{type B}) = 3.3 \times 10^{-6}$ GHz].

One sees that for large C_g the loaded quality factor follows a C_g^{-2} trend in agreement with equations (7) and (8). For smaller coupling capacitance Q_L

approaches a constant value. Below $C_g \sim 2$ fF, the contribution of Q_C to the loaded quality factor Q_L is negligible. The fact that Q_L increases with frequency at low capacitance, suggests that in this regime residual losses are dominant. Thus even weaker coupling than in our experiments would be desirable if one wants to achieve the highest possible Q_L that is only limited by the residual losses.

6. Discussion

To finish this study, we give some general remarks. As can be seen in figure 3 for lowest temperatures, the measured quality factor in dependence of frequency does not completely coincide with the fit, but the data are somewhat scattered. This scattering could be well reproduced when the resonators were measured twice in separate cooldowns. This would suggest that the scattering of the quality factor is due to some feature related to the resonator fabrication or its design. As an example, how critical elements of the resonator geometry are challenging to control precisely with our fabrication procedures, the length of the two coupling gaps can differ by 10% (see the photograph in figure 2(b)), whereas the model assumes perfect symmetry. Finally, as we make use of a lumped model for the coupled resonator, the parameters of the model are taken frequency independent except the resistance R . In other words, we assumed that in first order we can attribute all the frequency dependence of Q_L to the specific features we addressed in this study, although there could possibly exist other mechanisms that could play a role.

7. Conclusions

This study addresses how three different loss mechanisms govern the overall loaded quality factor of superconducting resonators: coupling to environment, thermal quasiparticles, and residual losses. For a given resonator design, the dominant loss mechanism depends on temperature and frequency, as illustrated by figure 1. We have verified this overall evolution experimentally using five stripline resonators fabricated from superconducting Pb, which differ in geometric dimensions, in particular concerning their coupling capacitance to the connecting microwave lines. In contrast to most studies on planar superconducting resonators, we have explicitly evaluated the frequency dependence by probing several harmonic modes, and there we have demonstrated the transition from Q_L dominated by residual losses at low frequencies to Q_L dominated by coupling losses at high frequencies, with a maximum Q_L at the transition between these ranges.

This work also concerns the potential of Pb as

superconducting material for planar microwave resonators. The electrodynamic properties of superconducting Pb were studied previously at microwave frequencies e.g. in the context of three-dimensional cavity resonators [44, 56–58], but there are comparably few studies that employ Pb for planar resonators [17, 37, 47, 59]. Our study shows Q_L around 200.000 for a temperature of 1.5 K, and following our investigation, this value could be easily exceeded if the coupling would be substantially weakened. This might be difficult to achieve for stripline resonators, and thus future studies might investigate Pb-based coplanar or lumped element resonators. Another open question concerns the power dependence: our work addresses resonator performance at temperatures above 1.5 K and at intermediate microwave powers around -40 dBm, as commonly employed in microwave spectroscopy. A different field of applications, quantum circuits, on the other hand typically works at much lower temperatures and at power levels corresponding to single photons [2, 11]. There the ‘residual losses’ play a different role than in our study, and thus it would be of interest to see how Pb resonators behave in that regime of lower temperatures and powers.

Acknowledgments

We thank Ioan Pop, Benjamin Sacépé, and Thibault Charpentier for helpful discussions. We acknowledge support by the State Graduate Support Program (Landesgraduiertenförderung) of Baden-Württemberg and by the BMBF within the project QSolid (FKZ: 13N16159).

Appendix A. Calculating the transition between regimes dominated by residual losses and thermal quasiparticles

The dashed curve in figure 1 at temperatures close to T_c and low frequencies that indicates the transition between the regime dominated by residual losses and the regime dominated by losses due to thermally excited quasiparticles, $Q_{QP} \sim Q_{Res}$, was computed via setting [60]

$$\begin{aligned} \frac{Q_{QP}}{Q_{Res}} &= \frac{Q_{QP}}{0.005 \cdot Q_N} = \frac{R_{S,N}}{0.005 \cdot R_{S,QP}} \\ &= \frac{1}{0.005} \cdot \operatorname{Re} \left[\sqrt{\frac{\hat{\sigma}_{QP}}{\hat{\sigma}_n}} \right], \end{aligned} \quad (13)$$

where R_S is the real part of the surface impedance and $\hat{\sigma}$ the optical conductivity, the subscript N denotes the normal conducting state. The ratio 0.005 between residual losses and normal state losses Q_N aligns with our results. The optical conductivity

of the quasiparticles $\hat{\sigma}_{QP}/\hat{\sigma}_n$ was computed via the Zimmermann formula in the dirty limit [61]. By using the Zimmermann formula we attribute the quasiparticle losses to low-frequency absorption due to thermally excited quasiparticles and to photon-induced pair-breaking excitations above the superconducting energy gap $\Delta(T)$ of the superconducting condensate. In that sense we assume that there are no quasiparticle losses at lowest temperature since we probe our resonator at frequencies $hf \ll 2\Delta_0$.

Appendix B. Fitting the temperature-dependent quasiparticle losses

The fits in figure 4(b) use as fit function for the expected temperature dependence of R_S [55]:

$$R_S \propto \frac{(\hbar\omega)^2}{k_B T} \ln \left\{ \frac{4k_B T}{\hbar\omega} \right\} \exp \left\{ -\frac{\Delta(T)}{k_B T} \right\} \quad (14)$$

with k_B the Boltzmann constant. For the temperature dependence of the superconducting energy gap $\Delta(T)$ we use the following approximation [62, 63]:

$$\frac{\Delta(T)}{\Delta_0} = \sqrt{\cos \left\{ \frac{\pi}{2} \left(\frac{T}{T_c} \right)^2 \right\}} \quad (15)$$

The fit parameters are $T_c = 6.7$ K (both curves) and $2\Delta_0/k_B T_c = 4.5$ (upper curve) and $2\Delta_0/k_B T_c = 4.8$ (lower curve). These values exceed the weak-coupling BCS value of $2\Delta_0/k_B T_c = 3.53$, which is consistent with previous reports of Pb being a strong coupling superconductor [64].

References

- [1] Göppl M *et al.* Coplanar waveguide resonators for circuit quantum electrodynamics. *J. Appl. Phys.*, 104:113904, 2009.
- [2] Zmuidzinas J. Superconducting Microresonators: Physics and Applications. *Annu. Rev. Condens. Matter Phys.*, 3:169–214, 2012.
- [3] Wallraff A, Schuster D, Blais A, Frunzio L, R-S Huang, Majer J, Kumar S, Girvin S, and Schoelkopf R. Strong coupling of a single photon to a superconducting qubit using circuit quantum electrodynamics. *Nature*, 431:162–167, 2004.
- [4] Frunzio L, Wallraff A, Schuster D, Majer J, and Schoelkopf R. Fabrication and characterization of superconducting circuit qed devices for quantum computation. *IEEE Trans. Appl. Supercond.*, 15:860–863, 2005.
- [5] Day P K, LeDuc H G, Mazin B A, Vayonakis A, and Zmuidzinas J. A broadband superconducting detector suitable for use in large arrays. *Nature*, 425:817–821, 2003.
- [6] Leduc H G *et al.* Titanium nitride films for ultrasensitive microresonator detectors. *Appl. Phys. Lett.*, 97:102509, 2010.
- [7] Moshe A G, Farber E, and Deutscher G. Granular superconductors for high kinetic inductance and low loss quantum devices. *Appl. Phys. Lett.*, 117:062601, 2020.

- [8] Samkharadze N, Bruno A, Scarlino P, Zheng G, DiVincenzo D P, DiCarlo L, and Vandersypen L M K. High-Kinetic-Inductance Superconducting Nanowire Resonators for Circuit QED in a Magnetic Field. *Phys. Rev. Appl.*, 5:044004, 2016.
- [9] Rotzinger H, Skacel S T, Pfirrmann M, Voss J N, Münzberg J, Probst S, Bushev P, Weides M P, Ustinov A V, and Mooij J E. Aluminium-oxide wires for superconducting high kinetic inductance circuits. *Supercond. Sci. Technol.*, 30:025002, 2016.
- [10] Grünhaupt L, Maleeva N, Skacel S T, Calvo M, Levy-Bertrand F, Ustinov A V, Rotzinger H, Monfardini A, Catelani G, and Pop M. Loss Mechanisms and Quasiparticle Dynamics in Superconducting Microwave Resonators Made of Thin-Film Granular Aluminum. *Phys. Rev. Lett.*, 121:117001, 2018.
- [11] Megrant A *et al.* Planar superconducting resonators with internal quality factors above one million. *Appl. Phys. Lett.*, 100:113510, 2012.
- [12] McRae C R H, Wang H, Gao J, Vissers M R, Brecht T, Dunswoth A, Pappas D P, and Mutus J. Materials loss measurements using superconducting microwave resonators. *Rev. Sci. Instrum.*, 91:091101, 2020.
- [13] Crowley *et al.* Disentangling Losses in Tantalum Superconducting Circuits. *Phys. Rev. X*, 13:041005, 2023.
- [14] DiIorio M S, Anderson A C, and Tsaun B Y. RF surface resistance of Y-Ba-Cu-O thin films. *Phys. Rev. B*, 38:7019–7022, 1988.
- [15] Oates D E, Anderson A C, Chin C C, Derov J S, Dresselhaus G, and Dresselhaus M S. Surface-impedance measurements of superconducting NbN films. *Phys. Rev. B*, 43:7655–7663, 1991.
- [16] Scheffler M *et al.* Microwave spectroscopy on heavy-fermion systems: Probing the dynamics of charges and magnetic moments. *Phys. Status Solidi B*, 250:439–449, 2013.
- [17] Hafner D, Dressel M, and Scheffler M. Surface-resistance measurements using superconducting stripline resonators. *Rev. Sci. Instrum.*, 85:014702, 2014.
- [18] Javaheri Rahim M, Lehleiter T, Bothner D, Krellner C, Koelle D, Kleiner R, Dressel M, and Scheffler M. Metallic coplanar resonators optimized for low-temperature measurements. *J. Appl. Phys.*, 49:395501, 2016.
- [19] Engl V T, Ebensperger N G, Wendel L, and Scheffler M. Planar GHz resonators on SrTiO_3 : Suppressed losses at temperatures below 1 K. *arXiv*, cond-mat.suprcon:1911.11456, 2019.
- [20] Langley B W, Anlage S M, Pease R F W, and Beasley M R. Magnetic penetration depth measurements of superconducting thin films by a microstrip resonator technique. *Rev. Sci. Instrum.*, 62:1801–1812, 1991.
- [21] Salluzzo M, Palomba F, Pica G, Andreone A, Maggio-Aprile I, Fischer Ø, Cantoni C, and Norton D P. Role of Nd/Ba disorder on the penetration depth of $\text{Nd}_{1+x}\text{Ba}_{2-x}\text{Cu}_3\text{O}_{7-\delta}$ thin films. *Phys. Rev. Lett.*, 85:1116–1119, 2000.
- [22] Driessen E F C, Coumou P C J J, Tromp R R, de Visser P J, and Klapwijk T M. Strongly disordered tin and nbn tin s -wave superconductors probed by microwave electrodynamic. *Phys. Rev. Lett.*, 109:107003, 2012.
- [23] Žemlička M *et al.* Finite quasiparticle lifetime in disordered superconductors. *Phys. Rev. B*, 92:224506, 2015.
- [24] Feller J R, Tsai C C, Ketterson J B, Smith J L, and Sarma Bimal K. Evidence of electromagnetic absorption by collective modes in the heavy fermion superconductor UBe_{13} . *Phys. Rev. Lett.*, 88:247005, 2002.
- [25] Truncik C J S *et al.* Nodal quasiparticle dynamics in the heavy fermion superconductor CeCoIn_5 revealed by precision microwave spectroscopy. *Nat. Commun.*, 4:2477, 2013.
- [26] Thiemann M *et al.* Single-gap superconductivity and dome of superfluid density in Nb-doped SrTiO_3 . *Phys. Rev. Lett.*, 120:237002, 2018.
- [27] Revenaz S, Oates D E, Labbé-Lavigne D, Dresselhaus G, and Dresselhaus M S. Frequency dependence of the surface impedance of $\text{YBa}_2\text{Cu}_3\text{O}_{7-\delta}$ thin films in a dc magnetic field: Investigation of vortex dynamics. *Phys. Rev. B*, 50:1178–1189, 1994.
- [28] Powell J R, Porch A, Humphreys R G, Wellhöfer F, Lancaster M J, and Gough C E. Field, temperature, and frequency dependence of the surface impedance of $\text{YBa}_2\text{Cu}_3\text{O}_7$ thin films. *Phys. Rev. B*, 57:5474–5484, 1998.
- [29] Ghirri A, Bonizzoni C, Gerace D, Sanna S, Cassinese A, and Affronte M. $\text{YBa}_2\text{Cu}_3\text{O}_7$ microwave resonators for strong collective coupling with spin ensembles. *Appl. Phys. Lett.*, 106:184101, 2015.
- [30] Velluire-Pellat Z *et al.* Hybrid quantum systems with high- T_c superconducting resonators. *Sci. Rep.*, 13:14366, 2023.
- [31] Ghigo G *et al.* Microwave dissipation in YBCO coplanar resonators with uniform and non-uniform columnar defect distribution. *Supercond. Sci. Technol.*, 17:977, 2004.
- [32] Levy-Bertrand F *et al.* Electrodynamics of granular aluminum from superconductor to insulator: Observation of collective superconducting modes. *Phys. Rev. B*, 99:094506, 2019.
- [33] Scheffler M *et al.* Broadband Corbino spectroscopy and stripline resonators to study the microwave properties of superconductors. *Acta IMEKO*, 4 (3):47-52, 2015.
- [34] Ghigo G, Ummarino G A, Gozzelino L, and Tamegai T. Penetration depth of $\text{Ba}_{1-x}\text{K}_x\text{Fe}_2\text{As}_2$ single crystals explained within a multiband Eliashberg $s \pm$ approach. *Phys. Rev. B*, 96:014501, 2017.
- [35] Ebensperger N G, Ferdinand B, Koelle D, Kleiner R, Dressel M, and Scheffler M. Characterizing dielectric properties of ultra-thin films using superconducting coplanar microwave resonators. *Rev. Sci. Instrum.*, 90:114701, 2019.
- [36] Ghigo G *et al.* Vortex dynamics in NbTi films at high frequency and high DC magnetic fields. *Sci. Rep.*, 13:9315, 2023.
- [37] Scheffler M, Fella C, and Dressel M. Stripline resonators for cryogenic microwave spectroscopy on metals and superconductors. *J. Phys. Conf. Ser.*, 400:052031, 2012.
- [38] Richards P L and Tinkham M. Far-Infrared Energy Gap Measurements in Bulk Superconducting In, Sn, Hg, Ta, V, Pb, and Nb. *Phys. Rev.*, 119:575–590, 1960.
- [39] Giaever I. Energy Gap in Superconductors Measured by Electron Tunneling. *Phys. Rev. Lett.*, 5:147–148, 1960.
- [40] Palmer L H and Tinkham M. Far-Infrared Absorption in Thin Superconducting Lead Films. *Phys. Rev.*, 165:588–595, 1968.
- [41] Klein O, Nicol E J, Holczer K, and Grüner G. Conductivity coherence factors in the conventional superconductors Nb and Pb. *Phys. Rev. B*, 50:6307–6316, 1994.
- [42] Ruby M, Heinrich B W, Pascual J I, and Franke K J. Experimental Demonstration of a Two-Band Superconducting State for Lead Using Scanning Tunneling Spectroscopy. *Phys. Rev. Lett.*, 114:157001, 2015.
- [43] Gozłinski T, Li Q, Heid R, Nemoto R, Willa R, Yamada T K, Schmalian J, and Wulfhkel W. Band-resolved Caroli–de Gennes–Matricon states of multiple-flux-quanta vortices in a multiband superconductor. *Sci. Adv.*, 9:eadh9163, 2023.
- [44] Pierce J M. Residual microwave surface resistance of superconducting lead. *J. Appl. Phys.*, 44:1342–1347, 1973.

- [45] Judish J P, Jones C M, McGowan F K, Milner W T, and Peebles P Z. Measurements of the low-temperature rf surface resistance of lead at frequencies from 136 to 472 MHz. *Phys. Rev. B*, 15:4412–4424, 1977.
- [46] Thakoor S, Strayer D M, Dick G J, and Mercereau J E. A lead-on-sapphire superconducting cavity of superior quality. *J. Appl. Phys.*, 59:854–858, 1986.
- [47] Ebensperger N G, Thiemann M, Dressel M, and Scheffler M. Superconducting Pb stripline resonators in parallel magnetic field and their application for microwave spectroscopy. *Supercond. Sci. Technol.*, 29:115004, 2016.
- [48] Thiemann M, Dressel M, and Scheffler M. Complete electrodynamics of a BCS superconductor with μeV energy scales: Microwave spectroscopy on titanium at mK temperatures. *Phys. Rev. B*, 97:214516, 2018.
- [49] Beydeda C *et al.* Characterization of harmonic modes and parasitic resonances in multi-mode superconducting coplanar resonators. *AIP Adv.*, 13:105027, 2023.
- [50] Pozar D M. *Microwave Engineering*. John Wiley & Sons, Inc., 2011.
- [51] Mattis D C and Bardeen J. Theory of the Anomalous Skin Effect in Normal and Superconducting Metals. *Phys. Rev.*, 111:412–417, 1958.
- [52] Cohn S B. Shielded coupled-strip transmission line. *IRE Transactions on Microwave Theory and Techniques*, 3:29–38, 1955.
- [53] Collin R E. *Foundations for Microwave Engineering*. Wiley, 1992.
- [54] Rausch D S, Thiemann M, Dressel M, Bothner D, Koelle D, Kleiner R, and Scheffler M. Superconducting coplanar microwave resonators with operating frequencies up to 50 GHz. *J. Phys. D: Appl. Phys.*, 51:465301, 2018.
- [55] Dressel M and Grüner G. *Electrodynamics of Solids*. Cambridge University Press, 2002.
- [56] Wilson P B. Investigation of the Q of a superconducting microwave cavity. *Nucl. Instrum. Methods Phys. Res.*, 20:336–340, 1963.
- [57] Hahn H, Halama H J, and Foster E H. Measurement of the Surface Resistance of Superconducting Lead at 2.868 GHz. *J. Appl. Phys.*, 39:2606–2609, 1968.
- [58] Tsai C C, Feller J R, Sarma Bimal K, and Ketterson J B. Instrumentation for cryogenic microwave cavity resonance measurements. *Rev. Sci. Instrum.*, 75:3158–3163, 2004.
- [59] Köpke M and Weis J. Superconducting Pb as material for coplanar waveguide resonators on GaAs substrates. *Phys. C: Supercond. Appl.*, 506:143–145, 2014.
- [60] Klein O, Donovan S, Dressel M, and Grüner G. Microwave cavity perturbation technique: Part I: Principles. *Int. J. Infrared Millim. Waves*, 14:2423–2457, 1993.
- [61] Zimmermann W, Brandt E H, Bauer M, Seider E, and Genzel L. Optical conductivity of BCS superconductors with arbitrary purity. *Phys. C: Supercond. Appl.*, 183:99–104, 1991.
- [62] Sheahen T P. Rules for the energy gap and critical field of superconductors. *Phys. Rev.*, 149:368–370, 1966.
- [63] Šindler M, Tesař R, Koláček J, Skrbek L, and Šimša Z. Far-infrared transmission of a superconducting NbN film. *Phys. Rev. B*, 81:184529, 2010.
- [64] Carbotte J P. Properties of boson-exchange superconductors. *Rev. Mod. Phys.*, 62:1027–1157, 1990.